Journal of King Saud University – Science 35 (2023) 102538

HOSTED BY

Contents lists available at ScienceDirect

Journal of King Saud University – Science

journal homepage: www.sciencedirect.com

Original article

Influence of operational parameters and kinetics analysis on photocatalytic hydrolysis of ammonia borane for H_2 production used heterojunction $FeTiO_3/TiO_2$-decorated carbon nanofibers

Abdullah M. Al-Enizi [a], Ayman Yousef [b,*], Mohd Ubaidullah [a], Alamgir Karim [c], M.M. El-Halwany [d]

[a] Department of Chemistry, College of Science, King Saud University, Riyadh 11451, Saudi Arabia
[b] Department of Mathematics and Physics Engineering, Faculty of Engineering at Mataria, Helwan University, Cairo 11718, Egypt
[c] Department of Chemical & Biomolecular Engineering, University of Houston, Houston, TX, USA
[d] Engineering Mathematics and Physics Department, Faculty of Engineering, Mansoura University, El-Mansoura, Egypt

ARTICLE INFO

Article history:
Received 13 May 2022
Revised 6 December 2022
Accepted 31 December 2022
Available online 6 January 2023

Keywords:
Iron **T**itanate
Nanofibers
Ammonia **B**orane **C**omplex
Hydrogen
Electrospinning
Visible **L**ight

ABSTRACT

In this work, carbon nanofibers (CNFs) decorated with heterojunction iron titanate/titanate nanoparticles ($FeTiO_3/TiO_2$ NPs) were effectively prepared using electrospinning for use as a photocatalyst in the production of hydrogen (H_2) from ammonia borane (AB). The as-prepared $FeTiO_3/TiO_2$@CNFs exhibited strong photocatalytic activity for H_2 release from photohydrolysis of the AB when exposed to visible light. Under visible light illumination, the observed H_2 evolution over TiO_2@CNFs was 0.38 mol in 14 min, whereas over $FeTiO_3/TiO_2$@CNFs it was 2.97 mol. Using $FeTiO_3/TiO_2$@CNFs, H_2 generation was shown to be substantially higher under visible light irradiation (2.97 mol/14 min) than in the dark (1.87 mol/14 min). A mathematical model was used to predict the photocatalytic activity of $FeTiO_3/TiO_2$@CNFs. Different operational factors were used to verify the accuracy of the mathematical model; they included the impact of AB concentration, light intensity, reaction temperature, and catalyst dosage. The reaction rate constant and equilibrium concentration were measured experimentally and compared to those predicted by the model. A good correlation was obtained between the calculated and measured photocatalytic activity.

1. Introduction

Advancement of the hydrogen economy has raised awareness of solid hydrogen storage materials (Simagina et al., 2021). Amongst, Ammonia borane (NH_3BH_3, AB) has gained interest due to its low molecular weight (30.87 g/mol), high hydrogen content (19.6 wt %), and durability in solid and aqueous solutions at ambient conditions (Demirci 2017). If an appropriate catalytic material is utilized, H_2 could be easily released from AB. The following equation describes the catalytic hydrolysis:

$$NH_3BH_3 + 3H_2O \rightarrow NH_3 + H_3BO_3 + 3H_2\uparrow \quad (1)$$

The first evidence of AB photohydrolysis was published in 2012 by Ayman et al (Yousef et al., 2012a). Many investigations have been carried on since then, with the aim of releasing hydrogen from AB using photocatalytic materials of different types and compositions (Yousef et al., 2012b, Yousef et al., 2013, Yousef et al., 2015a, Song et al., 2021, Yan et al., 2021). The photohydrolysis process may release gravimetric hydrogen capacity in AB, similar to conventional hydrolysis, while light irradiation can limit ammonia formation (Simagina et al., 2021). Photocatalysis, a "green" technology, offers significant promise for producing green energy and environmental remediation by removing hazardous compounds and pathogens (Hoffmann et al., 1995). Recent years have seen much research on photocatalysts incorporating metal oxides, sulfides, halides, etc (Yousef et al., 2012c, Yousef et al., 2017a). However, it is still difficult to develop photocatalysts that are effective, long-lasting, inexpensive, and kind on the environment. Thus, researchers have placed a premium in recent years on finding ways to modify materials to increase their photocatalytic activity. **Recently, perovskite-type oxides have been presented as a potential photocatalytic material due to their visible**

* Corresponding author.
E-mail address: aymanyousef84@gmail.com (A. Yousef).
Peer review under responsibility of King Saud University.

Production and hosting by Elsevier

https://doi.org/10.1016/j.jksus.2022.102538
1018-3647/

light-driven characteristics (Moradi et al., 2021**). Amongst them, Iron titanate ($FeTiO_3$) is attractive because to its non-toxicity, cheapness, and chemical and physical stability (**Kim et al., 2009, Abdou and Fadl 2019**). It is used in a broad variety of electromagnetic, chemical catalysts, photocatalysts optoelectronic and device applications due to its low band gap (2.5–2.9 eV) (**Kim et al., 2009, Verma et al., 2014**). The presence of Fe in the TiO_2 lattice could be improving its band gap and crystallinity (**Moradi et al., 2021**).** Lee and his group developed a heterojunction of $FeTiO_3$ and TiO_2. The proposed photocatalyst was very effective in photodegrading organic molecules under UV light irradiation (Kim et al., 2009). Quang and etal (Truong et al., 2012), used a hydrothermal process to prepared heterojunction $FeTiO_3/TiO_2$ photocatalysts. The developed photocatalyst showed excellent photocatalytic activity in the conversion of CO_2 to CH_3OH under both visible and UV- light irradiation. Masoud Moradi etal (Moradi et al., 2021), mixed graphene oxide (GO) with $FeTiO_3$ to reduce the band gap and improve the shift in the visible light range. They found that visible light causes faster photodegradation of phenolic compounds than ultraviolet light. High photocatalytic activity in the degradation of phenolic compounds was observed after 240 min of solar light irradiation. Incorporating GO into $FeTiO_3$ improved visible light absorption with decreasing hole-electro recombination. As is well-known, the shape and structure of nanomaterials, which in turn impact their catalytic activity, are directly influenced by the technique of synthesis used (Yousef et al., 2017b). Previous studies shown that carbon nanofibers (CNFs) may easily capture and transport photo-induce charges during the photocatalytic process owing to their high electrical conductivity (Liu et al., 2008, Unalan et al., 2008). The fabrication of heterojunction $FeTiO_3/TiO_2$@CNFs and their photocatalytic activity toward AB photohydrolysis are reported for the first time in the current study. The electrospinning technique was used in the preparation of the photocatalyst. Good photocatalytic activity towards H_2 production from AB photohydrolysis was shown for the synthesized NFs

2. Experimental

Experimental part is available in supporting information.

3. Results and discussion

3.1. Morphology study

There are a variety of techniques for making NFs, but electrospinning is by far the most common. The produced NFs have an excellent nanofibrous structure (Yousef et al., 2015b, Al-Enizi et al., 2017, Al-Enizi et al., 2019, Al-Enizi et al., 2020). Electrospun

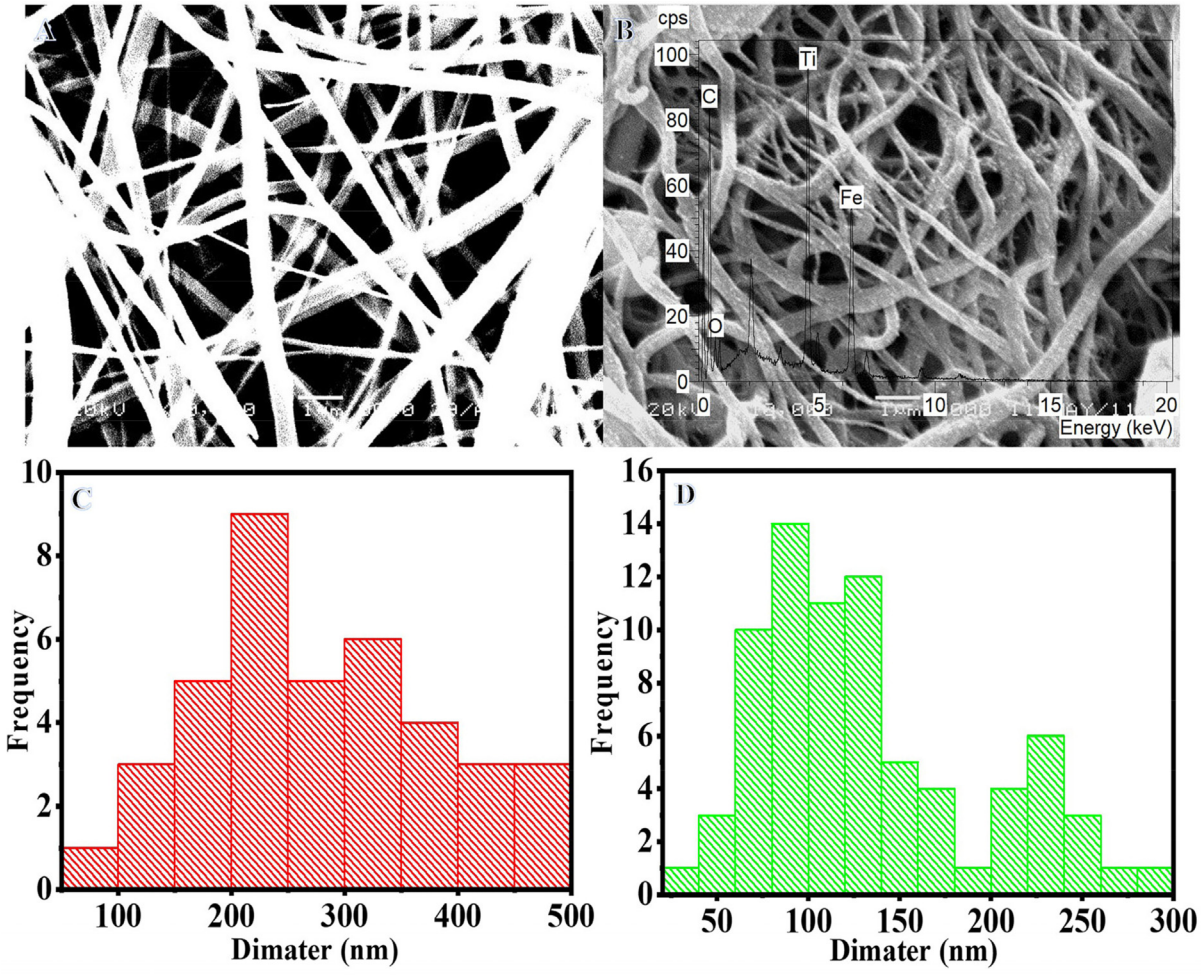

Fig. 1. SEM images of the electrospun FeAc/TIIP/PVP nanofiber mats after drying at 50 °C overnight (A) and the produced powder after calcination in Ar at 800 °C (B).

NF mats may have their nanofibrous structure preserved by sintering them at high temperatures in an inert atmosphere (Yousef et al., 2017c, Yousef et al., 2017d). Electrospun NF mats containing FeAc, TIIP, and PVP are shown in Sem image (Fig. 1**A**) after being vacuum dried at 50 °C overnight. The resulting NFs are shown to be smooth, continuous, and bead-free. Sintering at 800 °C for 5 h in an argon environment maintains the nanofibrous structure, which is an interesting finding (Fig. 1 **B**). In addition, tiny, white NPs may be seen growing on the surface of NFs. Due to polymer partial breakdown, the size of electrospun NF mats was significantly reduced during calcination, from 251.09 nm to 144.81 nm **(**Fig. 1**C and D).** EDX analysis (**Inset** Fig. 1**B**) reveals that iron (Fe), titanium (Ti), oxygen (O), and carbon (C) are the only elements present in the NFs.

3.2. Phase study

Fig. 2**A** displays the XRD patterns of the powder produced following the calcination process. According to the data, the formation of one peak from tetragonal TiO_2 rutile phase (JCPDS#21–1276) at 2θ value ~ 36.62° corresponds to (101). The hexagonal ilmenite $FeTiO_3$ phase (JCPDS#03–0781) has four peaks with 2θ value ~ 42.67°, 61.58°, 73.56°, and 77.63°, which are consistent with (202), (214), (217), and (223). In addition, a low intensity peak at a 2θ value ~ 26.1° is seen, which is associated with the (002) and suggests the synthesis of carbon-like graphite (Yousef et al., 2017a, 2017b, 2017c, 2017d, Xue et al., 2021). **The crystallite diameters of $FeTiO_3$ and TiO_2 were determined using Scherrer's equation to be 4.56 and 5.19 nm, respectively.** Fig. 2**B** shows a normal TEM image of the introduced NFs. Growth of NPs on the surface of NFs is easily visible in this image. The generated NPs might be $FeTiO_3/TiO_2$, whereas the NFs could be carbon. The HR-TEM image (**red circle in** Fig. 2**B**) displays a high crystalline structure with parallel atomic planes (Fig. 2**C**). Furthermore, distinct lattice fringes were identified in the sample, which might be related to the $FeTiO_3$ and/or TiO_2 phases. The production of polycrystalline material is shown in the SAED pattern of the designated region (**red circle in** Fig. 2**B**) seen in inset Fig. 2**C**. As demonstrated in Fig. 2**D**, the primary NFs are formed of amorphous structure (**blue circle in** Fig. 2**B**), suggesting the development of amorphous carbon. It may say that the NPs are crystalline $FeTiO_3/TiO_2$ NPs, while the NFs are amorphous carbon.

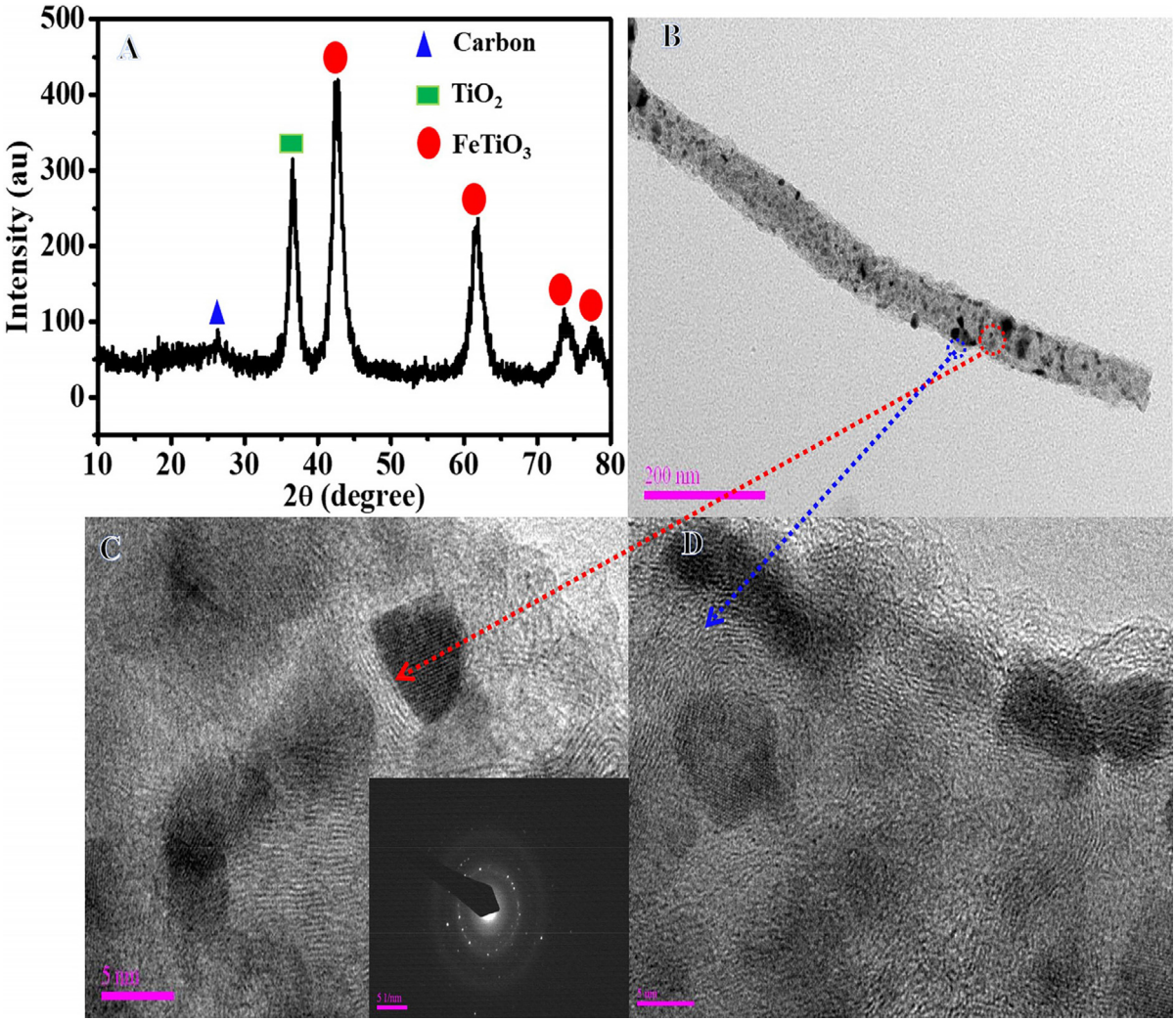

Fig. 2. XRD patterns (A), Normal TEM image of single NF (B) and HR-TEM images (C, D) of produced powder after calcination of electrospun FeAc/TIIP/PVP nanofiber mats at 800 °C in Ar atmosphere. The inset in Panel C represents the SAED of the marked area (red circle).

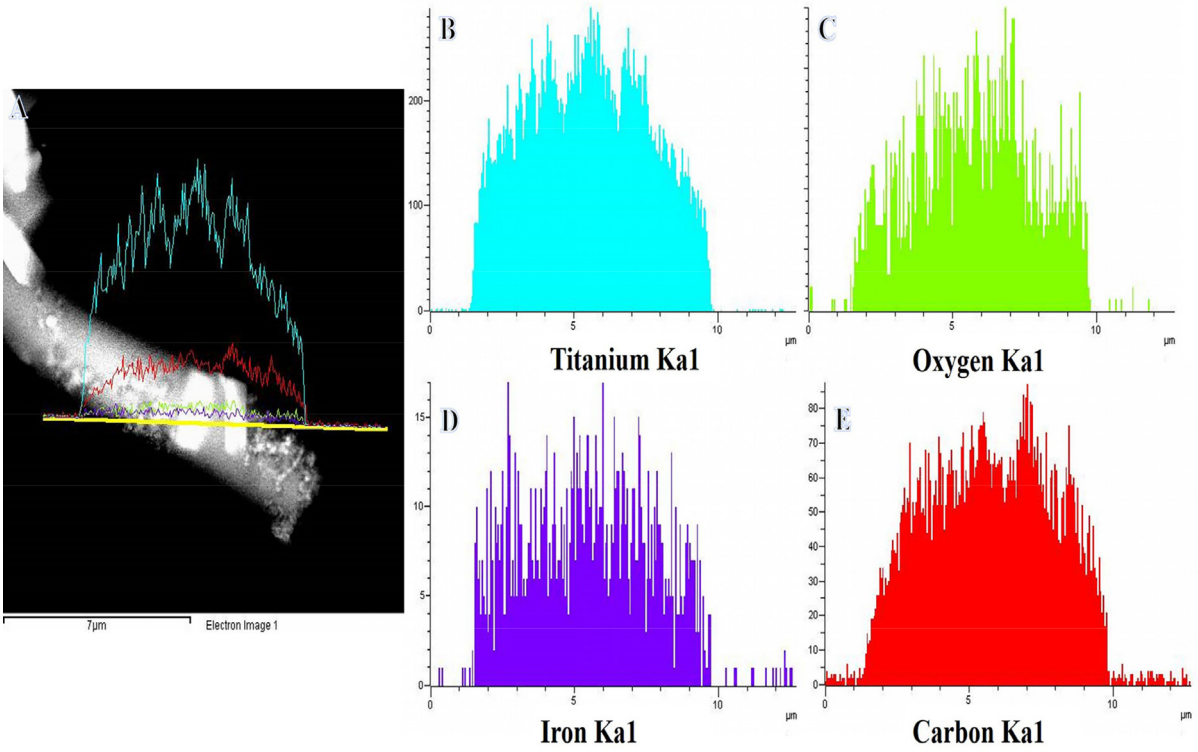

Fig. 3. TEM image of single NF along with the line TEM EDX analysis (A) and the corresponding Ti, O, Fe, and C line analyses TEM EDX (B, C, D).

TEM-EDX was utilized to determine the chemical composition of produced NFs (Fig. 3). Fig. 3**A** depicts a STEM image of a single chosen NF, as well as a line TEM-EDX analysis and the related EDX analysis, which are displayed in Fig. 3**B, C, D, and E**. The identical distributions of Ti, O, Fe, and C are observed, as illustrated in Figure, providing more evidence for the synthesis of $FeTiO_3$ and TiO_2. The addition of carbon to the phtocatalytic process may result in the following benefits: i) enhance photo-induced e^- and h^+ separation, and ii) enhance AB contact with the photocatalyst, via an adsorption process.

3.3. H_2 generation from the photohydrolysis of AB

At ambient temperature and under visible light irradiation (I = 25 Wm^{-2}), the photocatalytic activity of TiO_2@CNFs and $FeTiO_3/TiO_2$@CNFs was evaluated in terms of H_2 release from the hydrolysis of AB (1 mmol AB) (Fig. 4). The observed H_2 evolution over TiO_2@CNFs and $FeTiO_3/TiO_2$@CNFs were found to be 0.38 and 2.97 mmol in 14 min, respectively. FeTiO3/TiO2@CNFs displayed substantially greater activity than TiO_2@CNFs. This might be because to the quicker electro/hole separation on $FeTiO_3/TiO_2$@-CNFs, which improves H_2 production from AB photohydrolysis compared to TiO_2@CNFs. Also, H_2 generation was shown to be substantially higher in the presence of visible light than in the absence of it (Fig. 4). Even when exposed to visible light, no H_2 was detected in the absence of a photocatalyst, showing that AB was extremely stable in water. The effects of starting concentration (C_i), reaction temperature (T), photocatalyst dosage (CNFs), and light intensity (I) on the photocatalytic process have been investigated, and a mathematical model to predict these reactions has been developed (**Eq.S2**) (Ali et al., 2020):

3.3.1. Effect of initial AB concentration (C_i)

Under visible light irradiation, the influence of the initial AB concentration (0.1, 0.2, 0.3, and 0.4 M) on H_2 generation from AB photohydrolysis was studied (Fig. 5**A**). As indicated in the Figure, the initial H_2 production rate was relatively unaffected by the AB concentration. The photoproduction of H_2 at varying AB concentrations may be attributed to a pseudo-first order reaction, as described by the Langmuir Hinshelwood (LH) model (**Eq. S3**).

The relationship between ln C_i/C_f and reaction time is seen in Fig. 5**B**. Rate constants (K1) may be estimated from the slopes of

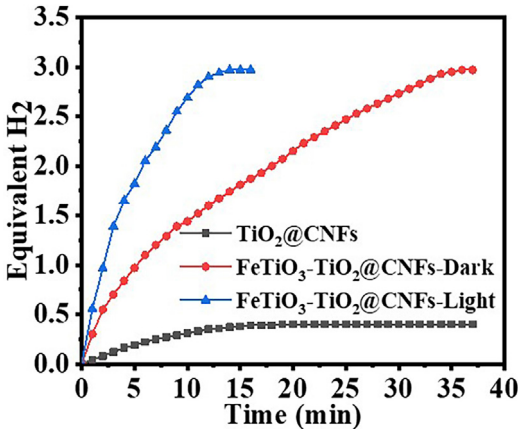

Fig. 4. H_2 generation in the presence of different photocatalysts. (Photocatalyst amount = 0.2 gm L-1, Ci = 0.1 M, T = 298 K, and I = 25 W m^{-2}).

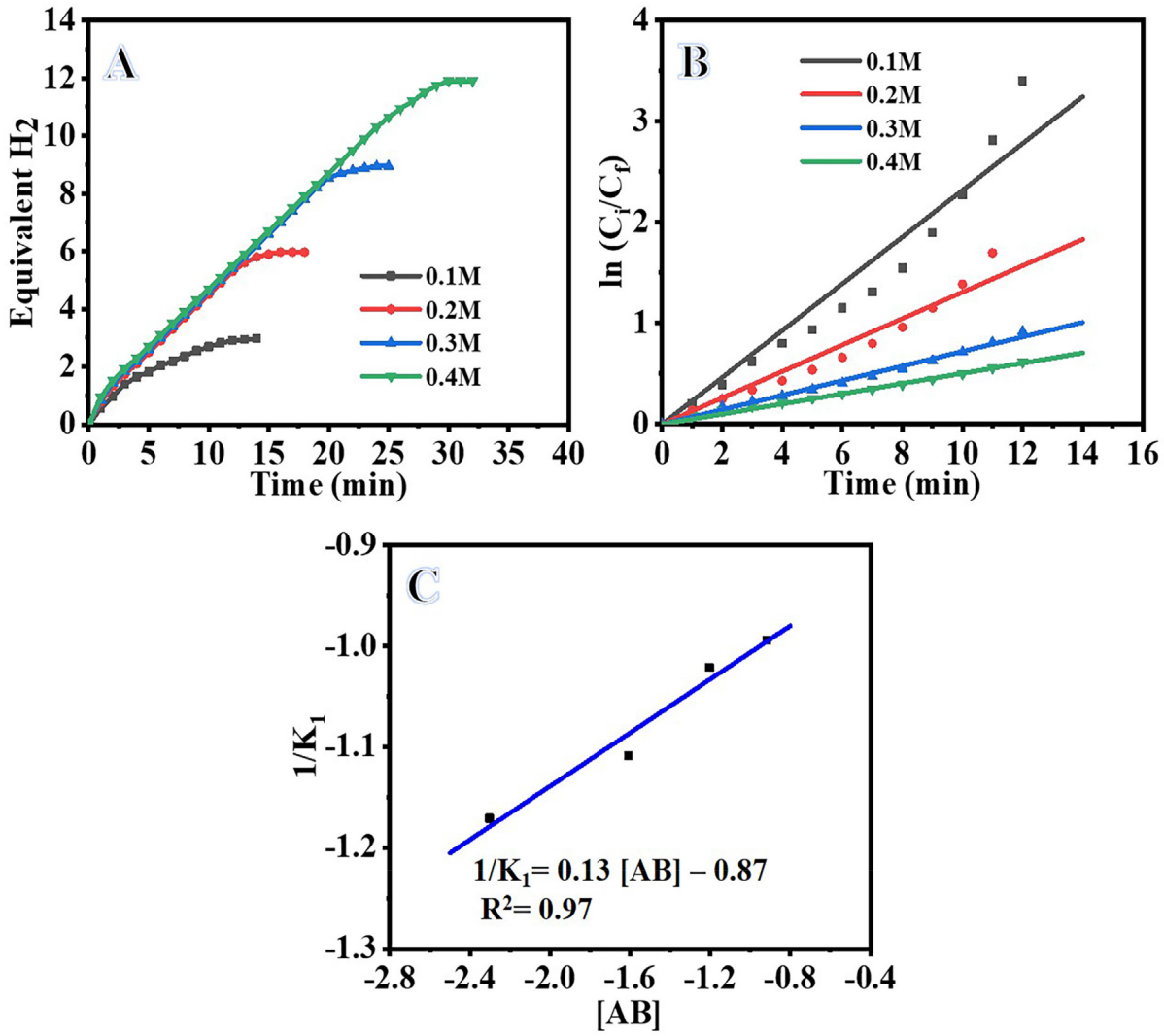

Fig. 5. Influence of [AB] on H_2 generation (A), ln Ci/Cf vs time (B), Modified LH plot for AB photohydrolysis (C). (Photocatalyst amount = 0.2 gm L-1, T = 298 K, and I = 25 W m^{-2}).

the straight lines shown in Fig. 5**B**. As [AB] increases from 0.1 to 0.4 M, K_1 decreases from 0.2318 to 0.0504 min^{-1} (**Table S1**). By transforming **Eq. S7** into a straight-line equation, we can determine the correlation between K_1 and initial [AB] (Fig. 5**C**).

3.3.2. *Effect of reaction temperature (T)*

The rate of H_2 production in the presence of $FeTiO_3/TiO_2$@CNFs vs irradiation time over a range of reaction temperatures is shown in Fig. 6**A**. Figure shows that when the reaction temperature is raised from 25 to 40 °C, photohydrolysis of AB increases due to enhanced charge carrier mobility and interfacial charge transfer. As the temperature of the reaction rises, photoelectron-hole pair movement increases, accelerating the interaction between adsorbed oxygen and electrons and between holes and OH radicals, speeding up AB photohydrolysis (Ojstršek et al., 2013, Meng et al., 2017, Chen and Hsu 2021). The kinetic analyses of AB photohydrolysis over $FeTiO_3/TiO_2$@CNFs at different temperatures are shown in Fig. 6**B**. Increases in the AB photohydrolysis efficiency with increasing temperature are shown by an increase in the reaction rate (K_2) from 0.2318 to 0.4148 min^{-1} as the reaction temperature increases from 25 to 40 °C (**Table S1**). A straight-line slope from Fig. 6**B** could be used to determine the rate constant (K_2). The plot of K_2 vs 1/T reveals a straight-line relationship (Fig. 6**C**). Using the Arrhenius equation (**Eq. S8**), we can get the activation energy (E_a) = 3.0162X10^4 of the photocatalytic process (Marandi et al., 2012). Applying the natural log to both sides of **Eq. S9** to remove the exponent.

3.3.3. *Effect of light intensity (I)*

Increases in light intensity increase the rate at which H_2 is produced by AB photohydrolysis (Wei et al., 2021). The influence of light intensity on AB photohydrolysis is shown in Fig. 7**A**. According to the results, the photohydrolysis rate of AB improved when the light intensity was increased. Enhanced AB photohydrolysis is likely due to an increase in the number of photons available per unit of time. The rate constant (K_3) could be determined from the slope of the straight lines produced from the plot of ln (H_2 generation rate) vs time (Fig. 7**B**) under varying light intensities. With

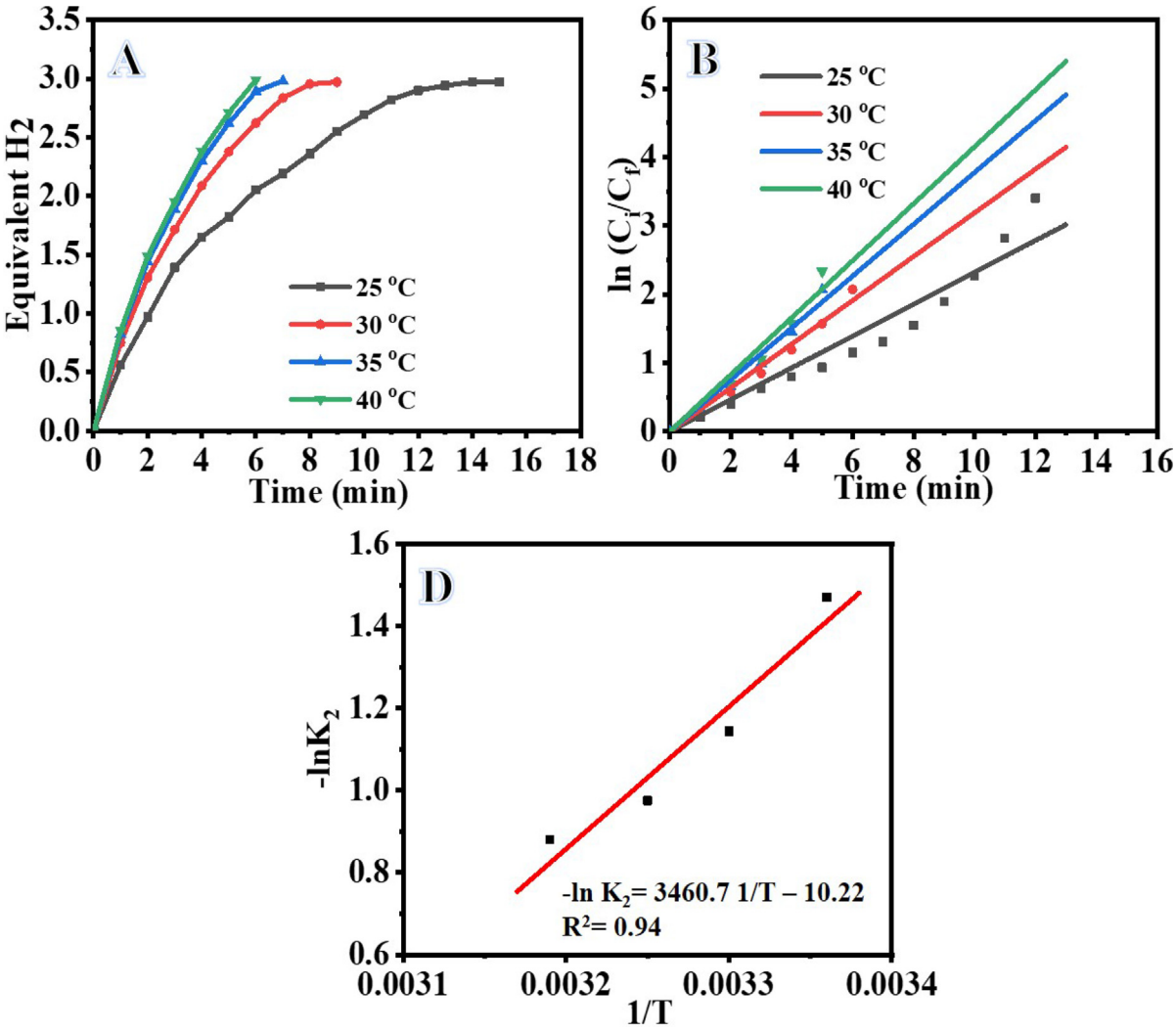

Fig. 6. Influence of Temperature on H_2 generation (A), ln C_i/C_f vs time (B), and (C) and Arrhenius plot for AB photohydrolysis. (Photocatalyst amount = 0.2 gm L^{-1}, C_i = 0.1 M, and I = 25 W m^{-2}).

an increase in light intensity, AB photohydrolysis increases, as shown by an increase in K_3 from 0.2318 to 0.3131 min^{-1} between 25 and 40 Wm^{-2} (**Table S1**). Since K_3 is directly proportional to I, we may determine their relationship by plotting $1/K_3$ vs I (Fig. 7**C**) and calculating for I using **Eq. S10.**

3.3.4. Effect of photocatalyst dose ($FeTiO_3/TiO_2$@CNFs)

H_2 production rate vs irradiation time for different $FeTiO_3/TiO_2$@CNFs concentrations (0.2, 0.3, 0.4, and 0.5 gm L^{-1}) is shown in Fig. 8**A**. Increases in the concentration of $FeTiO_3/TiO_2$@CNFs result in a higher rate of H_2 production, as indicated in the figure. This could be due to the increased surface area of the $FeTiO_3/TiO_2$@CNFs facilitates more efficient AB photohydrolysis. The kinetic studies over varying amounts of $FeTiO_3/TiO_2$@CNFs are shown in Fig. 8**B**. When the photocatalyst concentration is increasing from 0.2 to 0.5 gm L^{-1} (**Table S1**), the reaction rate (K_4) increases from 0.2318 to 0.5533 min^{-1}, showing an enhancement in the AB photohydrolysis. This may be because more adsorption and catalytic sites are available at the surface as a result of the higher concentration of $FeTiO_3/TiO_2$@CNFs. Fig. 8**C** illustrates the relationship between the logarithm of the reaction rate (K_4) and the logarithm of the dosage of [$FeTiO_3/TiO_2$@CNFs]. According to the best-fit line, the generated H_2 follows pseudo-first order kinetics in terms of catalyst concentration, with a slope of 0.9912. The Langmuir-type relationship (**Eq. S11**) (Ali et al., 2020) was used to determine how the $FeTiO_3/TiO_2$@CNFs concentration affected K_4 (Fig. 8**D**).This equation can be transforming to straight line equation (**Eq. S12**).

3.3.5. Development of model rate equation

According to **Equations (S7), (S9), (S10), and (S11)**, the rate constant is a function of the $FeTiO_3/TiO_2$@CNFs dose, AB concentration, light intensity, and reaction temperature. **Table S2** displays the calculated values of KR, Ea, m, and K_{NFs} using multiple regression analysis. The equation constant k' was calculated using **Eq. S2** by substituting the previous obtained values of C_i, T, I, C_{NFs} and values in **Table S2**, Kapp can be rewritten as follows:

$$K_{app} = K'\left(\frac{-29.52}{1 - 29.52 * 25_i}\right)\left(\exp\frac{-3.0162 * 10^4}{8.314 * 298}\right)(55 * 10^{-4} * 25)\left(\frac{0.34 * 0.2}{1 + 0.34 * 0.2}\right)$$

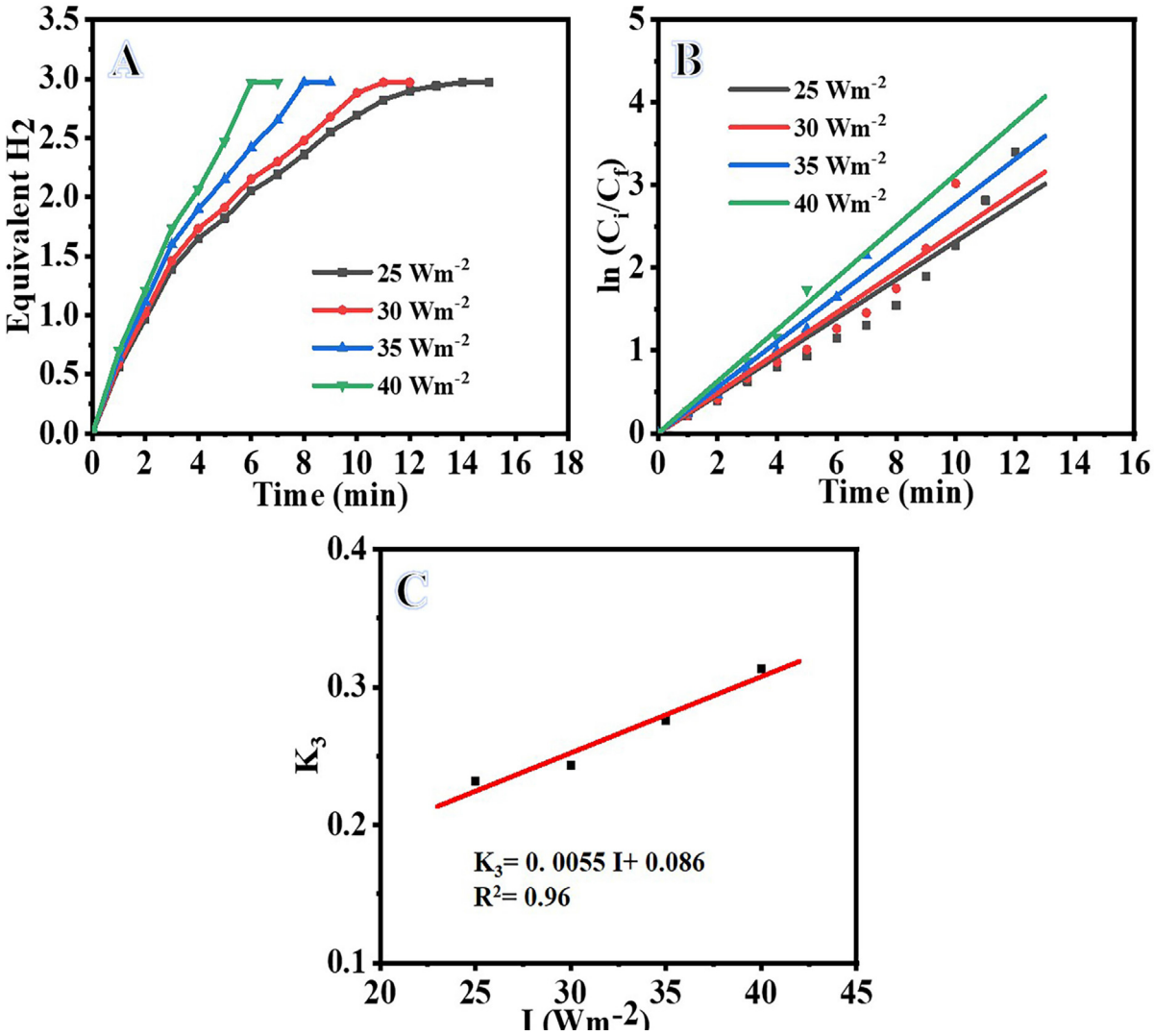

Fig. 7. Influence of light intensity on H_2 generation (A), ln C_i/C_f vs time (B), and logarithmic value of the H_2 generation vs logarithmic value of light intensity (C). (Photocatalyst amount = 0.2 gm L^{-1}, C_i = 0.1 M and T = 298 K).

$$0.2318 = K'\left(\frac{-29.52}{1 - 29.52 * 25_i}\right)\left(\exp\frac{-3.0162 * 10^4}{8.314 * 298}\right)(55 * 10^{-4} * 25)\left(\frac{0.34 * 0.2}{1 + 0.34 * 0.2}\right)$$

$$K' = 3.39 * 10^7$$

$$K_{app} = 3.39 * 10^7\left(\frac{-29.52}{1 - 29.52C_i}\right)\left(\exp\frac{-3.0162 * 10^4}{8.314T}\right)(55 * 10^{-4}I)\left(\frac{0.34C_{cat}}{1 + 0.34C_{cat}}\right)$$

Fig. 9 depicts a comparison of experimental data and determined Kapp for AB photohydrolysis under various conditions. The obtained plot demonstrated that the experimental data is in good agreement with the model calculated date, confirming the use of the model to predict the reaction rate constant under various operational conditions.

3.3.6. Photocatalytic mechanism

Producing active radicals is the first step in the photocatalytic process. The AB photohydrolysis method for H_2 generation over $FeTiO_3/TiO_2$@CNFs is shown in Fig. 10. Titanium dioxide, which has a band gap of 3.2 eV, is related to a limitation on the number of active radicals that may exist when illuminated by visible light (Kim et al., 2009). $FeTiO_3$ has a valence band (VB) potential of + 2.6 eV relative to a standard hydrogen electrode (SHE) and a conduction band (CB) potential of −0.2 eV (Moradi et al., 2021). The photogenerated positive hole (h +) combines with H_2O/OH^- to form hydroxyl radicals because the VB position of $FeTiO_3$ is so close to that of TiO_2 (+2.7 eV), allowing the hole to move from the VB of $FeTiO_3$ to that of TiO_2 (Moradi et al., 2021). With visible light irradiation, electrons in the CB of TiO_2 can be excited to $FeTiO_3$ CB, as shown in Fig. 10. This suggests that $FeTiO_3$ can be

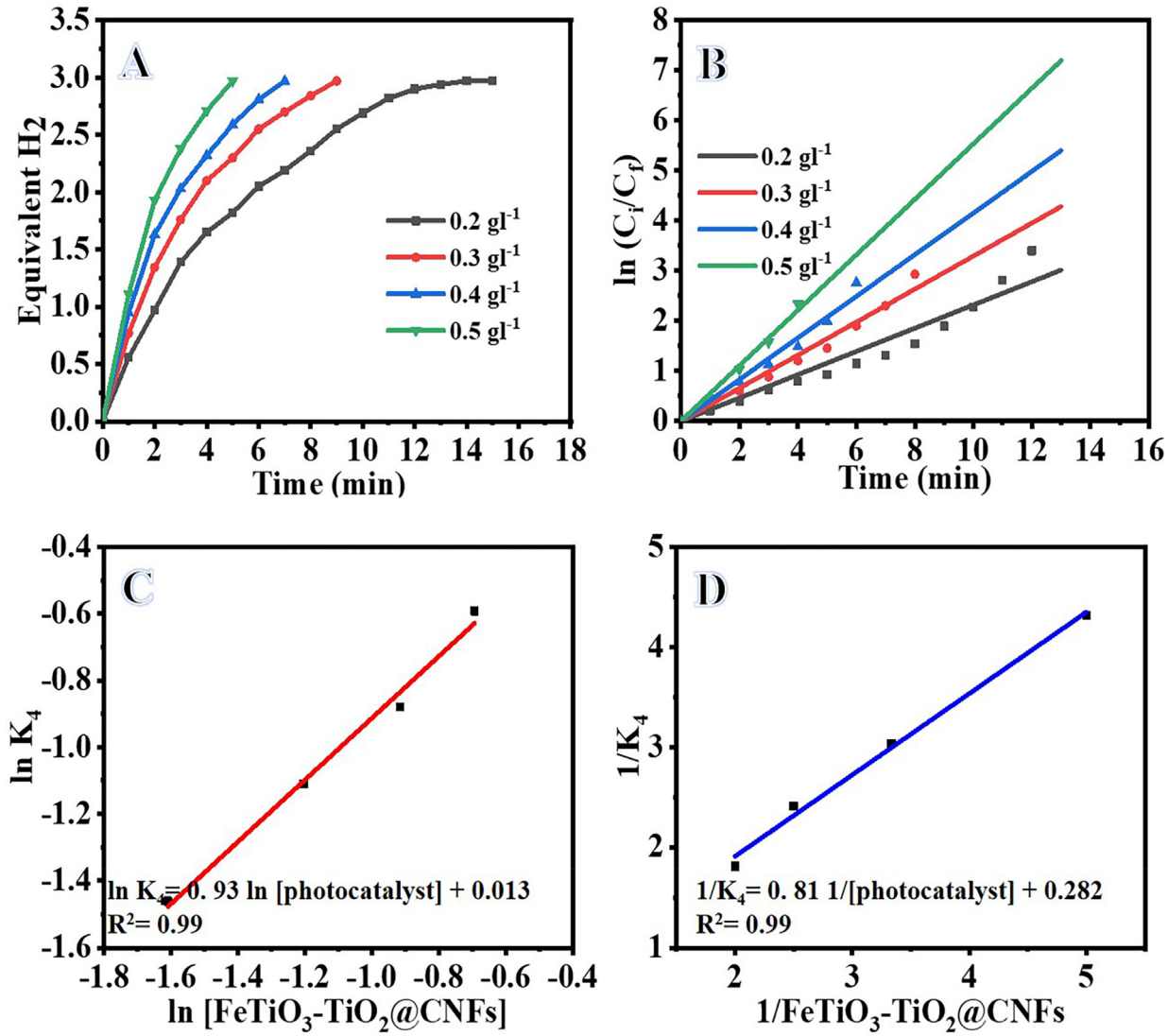

Fig. 8. Influence of catalyst amount on H_2 generation (A), ln Ci/Cf vs time (B), the logarithmic value of the H_2 generation rate vs logarithmic value of photocatalyst amount (C), and Langmuir-type plot for AB photohydrolysis (D). (C_i = 0.1 M, T = 298 K, and I = 25 W m^{-2}).

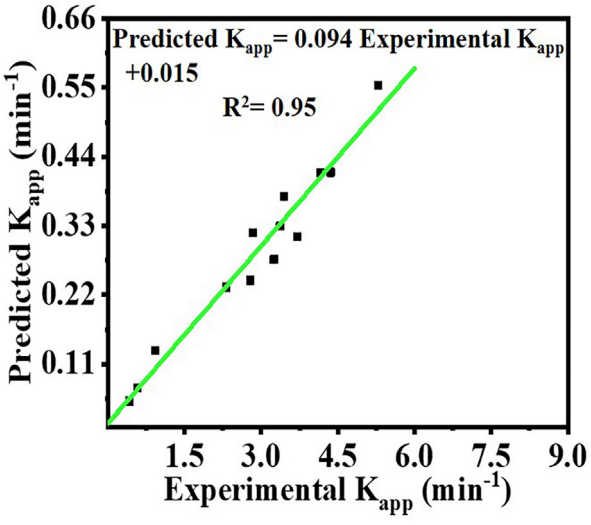

Fig. 9. Comparison of experimental kapp and predicted kapp values.

an effective sensitizer when exposed to visible light. Photogenerated electrons in $FeTiO_3$ move freely toward the surface of the CNFs, implying that photogenerated electrons and holes are efficiently separated due to low recombination (Zhang et al., 2012). Rather than recombination with holes on the surface of TiO_2, the photogenerated electron in the CB of $FeTiO_3$ can react with an oxidant such as an oxygen molecule (O_2) to produce $\cdot O^{2-}$.

4. Conclusion

Successfully preparation of heterojunction $FeTiO_3/TiO_2$@CNFs used electrospinning and calcination techniques. Under visible light, $FeTiO_3/TiO_2$@CNFs demonstrated fast hydrogen release via photohydrolysis of AB. The measured H_2 evolution over TiO_2@CNFs and $FeTiO_3/TiO_2$@CNFs were 0.38 mol and 0.97 mol in 14 min, respectively. This could be due to the faster electro/hole separation on $FeTiO_3/TiO_2$@CNFs, which improves H_2 generation from AB photohydrolysis over TiO_2@CNFs. It's worth noting that H_2 production increased significantly when exposed to visible light versus when exposed to darkness. The mathematical model predicts the reaction rate constant (k_{app}) by analyzing the effect of various

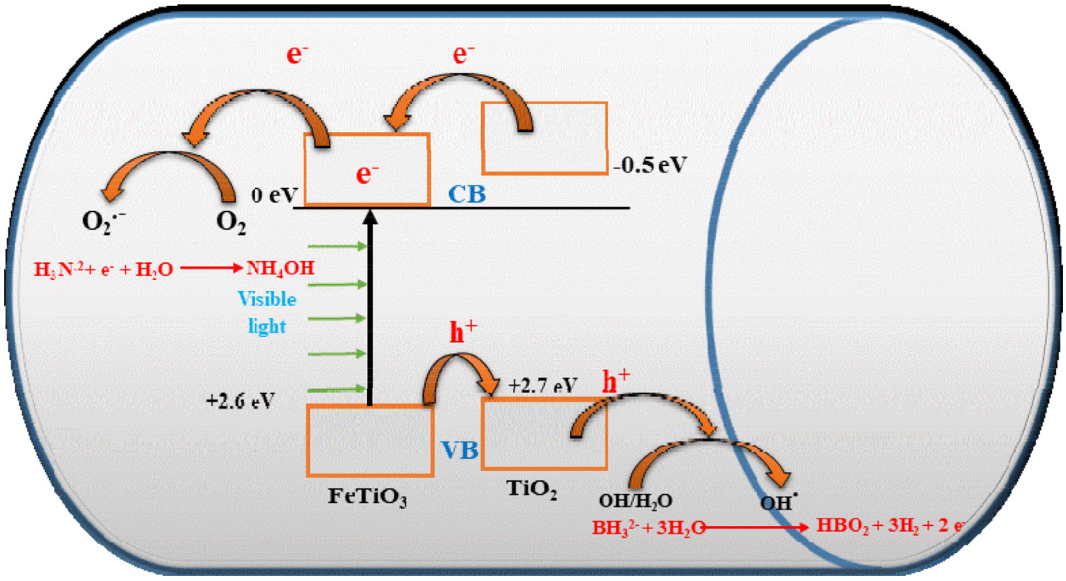

Fig. 10. Schematic diagram for the creation and influence of electrons and holes in the hydrolysis of the ammonia borane complex.

operational conditions. We observed that the experimental data agree well with the model-estimated data.

Declaration of Competing Interest

The authors declare that they have no known competing financial interests or personal relationships that could have appeared to influence the work reported in this paper.

Acknowledgements

The authors are grateful to be the Researchers supporting Project number (RSP-2022/55), King Saud University, Riyadh, Saudi Arabia for the support.

Appendix A. Supplementary material

Supplementary data to this article can be found online at https://doi.org/10.1016/j.jksus.2022.102538.

References

Abdou, M.I., Fadl, A.M., 2019. Assessment of nano-$FeTiO_3$/non crystalline silica cold galvanizing composite coating as a duplex corrosion guard system for steel electricity transmission towers in severe aggressive media. Constr. Build. Mater. 223, 705–723.

Al-Enizi, A.M., Brooks, R.M., Abutaleb, A., et al., 2017. Electrospun carbon nanofibers containing Co-TiC nanoparticles-like superficial protrusions as a catalyst for H_2 gas production from ammonia borane complex. Ceram. Int. 43, 15735–15742.

Al-Enizi, A.M., Nafady, A., El-Halwany, M., et al., 2019. Electrospun carbon nanofiber-encapsulated NiS nanoparticles as an efficient catalyst for hydrogen production from hydrolysis of sodium borohydride. Int. J. Hydrogen Energy 44, 21716–21725.

Al-Enizi, A.M., El-Halwany, M., Al-Abdrabalnabi, M.A., et al., 2020. Novel Low Temperature Route to Produce CdS/ZnO Composite Nanofibers as Effective Photocatalysts. Catalysts 10, 417.

Ali, I., Park, S., Kim, J.-O., 2020. Modeling the photocatalytic reactions of g-C_3N_4-TiO_2 nanocomposites in a recirculating semi-batch reactor. J. Alloy. Compd. 821, 153498.

Chen, Y.-W., Hsu, Y.-H., 2021. Effects of reaction temperature on the photocatalytic activity of TiO_2 with Pd and Cu cocatalysts. Catalysts 11, 966.

Demirci, U.B., 2017. Ammonia borane, a material with exceptional properties for chemical hydrogen storage. Int. J. Hydrogen Energy 42, 9978–10013.

Hoffmann, M.R., S.T. Martin, W. Choi, et al., 1995. Environmental applications of semiconductor photocatalysis. 95, 69-96.

Kim, Y.J., Gao, B., Han, S.Y., et al., 2009. Heterojunction of $FeTiO_3$ nanodisc and TiO_2 nanoparticle for a novel visible light photocatalyst. J. Phys. Chem. C 113, 19179–19184.

Liu, J., Li, J., Sedhain, A., et al., 2008. Structure and photoluminescence study of TiO_2 nanoneedle texture along vertically aligned carbon nanofiber arrays. J. Phys. Chem. C 112, 17127–17132.

Marandi, R., Olya, M.E., Vahid, B., et al., 2012. Kinetic modeling of photocatalytic degradation of an azo dye using nano-TiO_2/polyester. Environ. Eng. Sci. 29, 957–963.

Meng, Y., Xia, S., Pan, G., et al., 2017. Preparation and photocatalytic activity of composite metal oxides derived from Salen-Cu (II) intercalated layered double hydroxides. Korean J. Chem. Eng. 34, 2331–2341.

Moradi, M., Vasseghian, Y., Khataee, A., et al., 2021. Ultrasound-assisted synthesis of $FeTiO_3$/GO nanocomposite for photocatalytic degradation of phenol under visible light irradiation. Sep. Purif. Technol. 261, 118274.

Ojstršek, A., Kleinschek, K.S., Fakin, D., 2013. Characterization of nano-sized TiO_2 suspensions for functional modification of polyester fabric. Surf. Coat. Technol. 226, 68–74.

Simagina, V.I., Komova, O.V., Ozerova, A.M., et al., 2021. TiO_2-based photocatalysts for controllable hydrogen evolution from ammonia borane. Catal. Today 379, 149–158.

Song, J., Wu, F., Lu, Y., et al., 2021. $CeVO_4$/CeO_2 Heterostructure-Supported Co Nanoparticles for Photocatalytic H_2 Production from Ammonia Borane under Visible Light. ACS Applied Nano Materials. 4, 4800–4809.

Truong, Q.D., Liu, J.-Y., Chung, C.-C., et al., 2012. Photocatalytic reduction of CO_2 on $FeTiO_3$/TiO_2 photocatalyst. Catal. Commun. 19, 85–89.

Unalan, H.E., Wei, D., Suzuki, K., et al., 2008. Photoelectrochemical cell using dye sensitized zinc oxide nanowires grown on carbon fibers. Appl. Phys. Lett. 93, 133116.

Verma, N., Singh, S., Srivastava, R., et al., 2014. Fabrication of iron titanium oxide thin film and its application as opto-electronic humidity and liquefied petroleum gas sensors. Opt. Laser Technol. 57, 181–188.

Wei, L., Yang, Y., Yu, Y.-N., et al., 2021. Visible-light-enhanced catalytic hydrolysis of ammonia borane using RuP2 quantum dots supported by graphitic carbon nitride. Int. J. Hydrogen Energy 46, 3811–3820.

Xue, Z., Xiong, Q., Zou, C., et al., 2021. Growth of carbon nanofibers through chemical vapor deposition for enhanced sodium ion storage. Mater. Res. Bull. 133, 111049.

Yan, Y., Zhang, C., Jia, T., et al., 2021. Efficient hydrogen production by an rGO/TiO_2 composite material from ammonia borane hydrolysis in a photocatalytic reactor. Energy Fuel 35, 16065–16074.

Yousef, A., N. A. Barakat, K. A. Khalil, et al., 2012. Photocatalytic release of hydrogen from ammonia borane-complex using Ni (0)-doped TiO2/C electrospun nanofibers. 410, 59-65.

Yousef, A., Barakat, N.A.M., Al-Deyab, S.S., et al., 2012b. Encapsulation of CdO/ZnO NPs in PU electrospun nanofibers as novel strategy for effective immobilization of the photocatalysts. Colloids Surf. A Physicochem. Eng. Asp 401, 8–16.

Yousef, A., Barakat, N.A.M., Khalil, K.A., et al., 2012c. Photocatalytic release of hydrogen from ammonia borane-complex using Ni (0)-doped TiO_2/C electrospun nanofibers. Colloids Surf. A Physicochem. Eng. Asp 410, 59–65.

Yousef, A., Barakat, N.A.M., Kim, H.Y., 2013. Electrospun Cu-doped titania nanofibers for photocatalytic hydrolysis of ammonia borane. Appl. Catal. A 467, 98–106.

Yousef, A., El-Halwany, M., Barakat, N.A., et al., 2015a. Cu0-doped TiO_2 nanofibers as potential photocatalyst and antimicrobial agent. J. Ind. Eng. Chem. 26, 251–258.

Yousef, A., El-Halwany, M.M., Barakat, N.A.M., et al., 2015b. One pot synthesis of Cu-doped TiO_2 carbon nanofibers for dehydrogenation of ammonia borane. Ceram. Int. 41, 6137–6140.
Yousef, A., Brooks, R.M., Abutaleb, A., et al., 2017a. One-step synthesis of Co-TiC-carbon composite nanofibers at low temperature. Ceram. Int. 43, 5828–5831.
Yousef, A., Brooks, R.M., El-Halwany, M.M., et al., 2017b. Electrospun $CoCr7C_3$-supported C nanofibers: effective, durable, and chemically stable catalyst for H_2 gas generation from ammonia borane. Mol. Catal. 434, 32–38.
Yousef, A., Brooks, R.M., El-Newehy, M.H., et al., 2017c. Electrospun Co-TiC nanoparticles embedded on carbon nanofibers: Active and chemically stable counter electrode for methanol fuel cells and dye-sensitized solar cells. Int. J. Hydrogen Energy 42, 10407–10415.
Yousef, A., El-Halwany, M.M., El-Newehy, M.H., et al., 2017d. Synthesis of Cu–S-Codoped TiO_2 nanoparticles supported on carbon nanofibers for simultaneous adsorption and photocatalytic decomposition of reactive black 5. J. Nanosci. Nanotechnol. 17, 3998–4004.
Zhang, M., Shao, C., Mu, J., et al., 2012. Hierarchical heterostructures of Bi_2MoO_6 on carbon nanofibers: controllable solvothermal fabrication and enhanced visible photocatalytic properties. J. Mater. Chem. 22, 577–584.